Supporting Informatin

A gadolinium MOF acting as a multi-responsive and highly selective luminescent sensor for detecting *o*-, *m*- , *p*-nitrophenol and Fe^{3+} ions in aqueous phase

Qing-Hua Tan, Yan-Qin Wang,* Xiao-Yu Guo, Hou-Ting Liu and Zhi-Liang Liu*

Table S1. The selected bond lengths and angles for compound **1**.

Gd(1)-O(12)	2.292(8)	Gd(1)-O(5)A	2.312(8)
Gd(1)-O(3)	2.340(7)	Gd(1)-O(19)B	2.422(10)
Gd(1)-O(21)	2.436(10)	Gd(1)-O(7)C	2.435(9)
Gd(1)-O(8)C	2.476(8)	Gd(1)-O(20)B	2.472(7)
Gd(2)-O(10)	2.305(9)	Gd(2)-O(6)C	2.332(8)
Gd(2)-O(4)D	2.364(8)	Gd(2)-O(13)E	2.360(8)
Gd(2)-O(25)	2.436(7)	Gd(2)-O(17)	2.449(9)
Gd(2)-O(2)	2.491(8)	Gd(2)-O(18)	2.577(10)
Gd(2)-C(45)	2.861(15)	Gd(3)-O(14)E	2.268(9)
Gd(3)-O(9)	2.318(8)	Gd(3)-O(1)	2.330(8)
Gd(3)-O(24)	2.364(9)	Gd(3)-O(22)	2.429(12)
Gd(3)-O(15)F	2.398(9)	Gd(3)-O(23)	2.438(9)
Gd(3)-O(16)F	2.512(8)	Gd(3)-C(44)F	2.836(13)
O(4)-Gd(2)G	2.364(8)	O(5)-Gd(1)E	2.312(8)
O(6)-Gd(2)F	2.332(8)	O(7)-Gd(1)F	2.435(8)
O(8)-Gd(1)F	2.476(8)	O(13)-Gd(2)A	2.360(8)
O(14)-Gd(3)A	2.268(9)	O(15)-Gd(3)C	2.398(9)
O(16)-Gd(3)C	2.512(8)	O(19)-Gd(1)B	2.422(10)
O(20)-Gd(1)B	2.472(7)	O(12)-Gd(1)-O(5)A	94.2(3)
O(12)-Gd(1)-O(3)	79.1(3)	O(5)A-Gd(1)-O(3)	84.1(3)
O(12)-Gd(1)-O(19)B	157.7(3)	O(5)A-Gd(1)-O(19)B	86.1(3)
O(3)-Gd(1)-O(19)B	78.7(3)	O(12)-Gd(1)-O(21)	72.3(3)
O(5)A-Gd(1)-O(21)	77.2(4)	O(3)-Gd(1)-O(21)	144.3(3)
O(19)B-Gd(1)-O(21)	129.1(3)	O(12)-Gd(1)-O(7)C	87.4(3)

O(5)A-Gd(1)-O(7)C	157.8(3)	O(3)-Gd(1)-O(7)C	74.4(3)
O(19)B-Gd(1)-O(7)C	84.2(3)	O(21)-Gd(1)-O(7)C	124.0(3)
O(12)-Gd(1)-O(8)C	95.1(3)	O(5)A-Gd(1)-O(8)C	149.0(3)
O(3)-Gd(1)-O(8)C	126.7(3)	O(19)B-Gd(1)-O(8)C	96.1(3)
O(21)-Gd(1)-O(8)C	77.5(3)	O(7)C-Gd(1)-O(8)C	52.4(3)
O(12)-Gd(1)-O(20)B	149.0(3)	O(5)A-Gd(1)-O(20)B	79.2(3)
O(3)-Gd(1)-O(20)B	129.4(3)	O(19)B-Gd(1)-O(20)B	52.9(3)
O(8)C-Gd(1)-O(20)B	77.6(3)	O(12)-Gd(1)-C(52)B	173.0(4)
O(21)-Gd(1)-O(20)B	76.7(3)	O(7)C-Gd(1)-O(20)B	110.1(3)
O(5)A-Gd(1)-C(52)B	79.6(4)	O(3)-Gd(1)-C(52)B	103.3(4)
O(19)B-Gd(1)-C(52)B	26.3(3)	O(21)-Gd(1)-C(52)B	102.9(4)
O(7)C-Gd(1)-C(52)B	99.6(4)	O(8)C-Gd(1)-C(52)B	88.7(4)
O(20)B-Gd(1)-C(52)B	26.8(3)	O(12)-Gd(1)-C(22)C	91.0(4)
O(5)A-Gd(1)-C(22)C	173.9(3)	O(3)-Gd(1)-C(22)C	100.0(3)
O(19)B-Gd(1)-C(22)C	90.3(4)	O(21)-Gd(1)-C(22)C	101.4(4)
O(7)C-Gd(1)-C(22)C	25.7(3)	O(8)C-Gd(1)-C(22)C	26.7(3)
O(20)B-Gd(1)-C(22)C	94.7(3)	C(52)B-Gd(1)-C(22)C	95.0(4)
O(10)-Gd(2)-O(6)C	88.1(3)	O(10)-Gd(2)-O(4)D	138.6(3)
O(6)C-Gd(2)-O(4)D	85.4(3)	O(10)-Gd(2)-O(13)E	83.2(3)
O(6)C-Gd(2)-O(13)E	150.4(3)	O(4)D-Gd(2)-O(13)E	82.8(3)
O(10)-Gd(2)-O(25)	64.4(3)	O(6)C-Gd(2)-O(25)	76.8(3)
O(4)D-Gd(2)-O(25)	74.3(3)	O(13)E-Gd(2)-O(25)	74.0(3)
O(10)-Gd(2)-O(17)	134.1(3)	O(6)C-Gd(2)-O(17)	128.6(3)
O(4)D-Gd(2)-O(17)	78.4(3)	O(13)E-Gd(2)-O(17)	75.1(3)
O(25)-Gd(2)-O(17)	140.8(3)	O(10)-Gd(2)-O(2)	77.1(3)
O(6)C-Gd(2)-O(2)	77.1(3)	O(4)D-Gd(2)-O(2)	139.9(3)
O(13)E-Gd(2)-O(2)	127.6(3)	O(25)-Gd(2)-O(2)	133.6(3)
O(17)-Gd(2)-O(2)	84.9(3)	O(10)-Gd(2)-O(18)	146.5(3)
O(6)C-Gd(2)-O(18)	77.3(3)	O(4)D-Gd(2)-O(18)	70.8(3)
O(13)E-Gd(2)-O(18)	123.3(3)	O(25)-Gd(2)-O(18)	137.7(3)
O(17)-Gd(2)-O(18)	51.3(3)	O(2)-Gd(2)-O(18)	70.3(3)
O(10)-Gd(2)-C(45)	150.9(4)	O(6)C-Gd(2)-C(45)	103.1(4)
O(4)D-Gd(2)-C(45)	69.8(4)	O(13)E-Gd(2)-C(45)	98.1(4)
O(25)-Gd(2)-C(45)	144.0(4)	O(17)-Gd(2)-C(45)	25.7(3)

O(2)-Gd(2)-C(45)	79.4(3)	O(18)-Gd(2)-C(45)	26.0(3)
O(14)E-Gd(3)-O(9)	85.6(3)	O(14)E-Gd(3)-O(1)	85.7(3)
O(9)-Gd(3)-O(1)	77.4(3)	O(14)E-Gd(3)-O(24)	106.9(4)
O(9)-Gd(3)-O(24)	72.8(3)	O(1)-Gd(3)-O(24)	146.4(3)
O(14)E-Gd(3)-O(22)	77.6(4)	O(9)-Gd(3)-O(22)	145.7(4)
O(1)-Gd(3)-O(22)	71.7(4)	O(24)-Gd(3)-O(22)	140.7(4)
O(14)E-Gd(3)-O(15)F	146.8(3)	O(9)-Gd(3)-O(15)F	127.6(3)
O(1)-Gd(3)-O(15)F	102.4(3)	O(24)-Gd(3)-O(15)F	84.2(3)
O(22)-Gd(3)-O(15)F	74.7(4)	O(14)E-Gd(3)-O(23)	76.3(3)
O(9)-Gd(3)-O(23)	132.9(4)	O(1)-Gd(3)-O(23)	141.8(3)
O(24)-Gd(3)-O(23)	71.7(3)	O(22)-Gd(3)-O(23)	71.7(4)
O(15)F-Gd(3)-O(23)	77.9(3)	O(14)E-Gd(3)-O(16)F	160.2(3)
O(9)-Gd(3)-O(16)F	75.6(3)	O(1)-Gd(3)-O(16)F	84.4(3)
O(24)-Gd(3)-O(16)F	73.5(3)	O(22)-Gd(3)-O(16)F	115.1(4)
O(15)F-Gd(3)-O(16)F	52.6(3)	O(23)-Gd(3)-O(16)F	121.2(3)
O(14)E-Gd(3)-C(44)F	172.9(4)	O(9)-Gd(3)-C(44)F	101.4(3)
O(1)-Gd(3)-C(44)F	94.7(4)	O(24)-Gd(3)-C(44)F	76.6(4)
O(22)-Gd(3)-C(44)F	95.8(4)	O(15)F-Gd(3)-C(44)F	26.4(3)
O(23)-Gd(3)-C(44)F	99.4(4)	O(16)F-Gd(3)-C(44)F	26.3(3)
C(1)-O(1)-Gd(3)	144.1(8)	C(1)-O(2)-Gd(2)	112.1(8)
C(8)-O(3)-Gd(1)	153.4(8)	C(8)-O(4)-Gd(2)G	145.5(8)
C(21)-O(5)-Gd(1)E	175.5(10)	C(21)-O(6)-Gd(2)F	146.2(8)
C(22)-O(7)-Gd(1)F	95.2(7)	C(22)-O(8)-Gd(1)F	92.2(7)
C(30)-O(9)-Gd(3)	132.2(8)	C(30)-O(10)-Gd(2)	142.8(9)
C(23)-O(12)-Gd(1)	140.9(9)	C(43)-O(13)-Gd(2)A	138.2(8)
C(43)-O(14)-Gd(3)A	153.6(10)	C(44)-O(15)-Gd(3)C	96.5(8)
C(44)-O(16)-Gd(3)C	91.4(7)	C(45)-O(17)-Gd(2)	96.0(8)
C(45)-O(18)-Gd(2)	89.8(9)	C(52)-O(19)-Gd(1)B	93.9(9)
C(52)-O(20)-Gd(1)B	91.0(7)	O(7)-C(22)-Gd(1)F	59.1(7)
O(8)-C(22)-Gd(1)F	61.1(6)	C(19)-C(22)-Gd(1)F	177.0(9)
O(19)-C(52)-Gd(1)B	59.9(7)	O(20)-C(52)-Gd(1)B	62.2(7)
C(48)-C(52)-Gd(1)B	167.8(10)		

Symmetry transformations used to generate equivalent atoms: A: x,y+1,z; B: -x+1,-y+2,-z; C: x+1,y+1,z; D: x+1,y,z; E: x,y-1,z; F: x-1,y-1,z; G: x-1,y,z; H: -x+2,-y+1,-z.

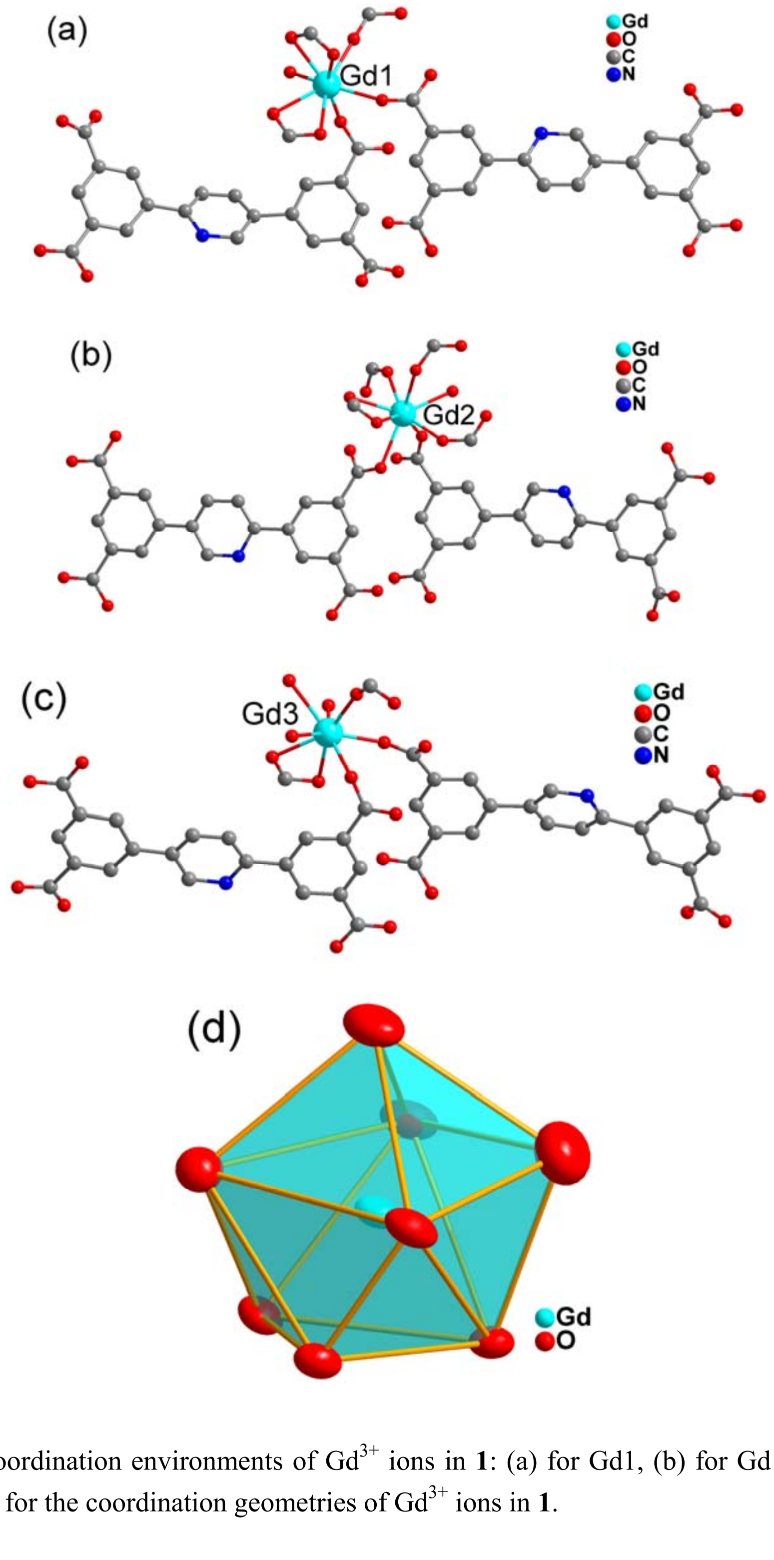

Fig. S1 The coordination environments of Gd^{3+} ions in **1**: (a) for Gd1, (b) for Gd 2, (c) for Gd3 and (d) for the coordination geometries of Gd^{3+} ions in **1**.

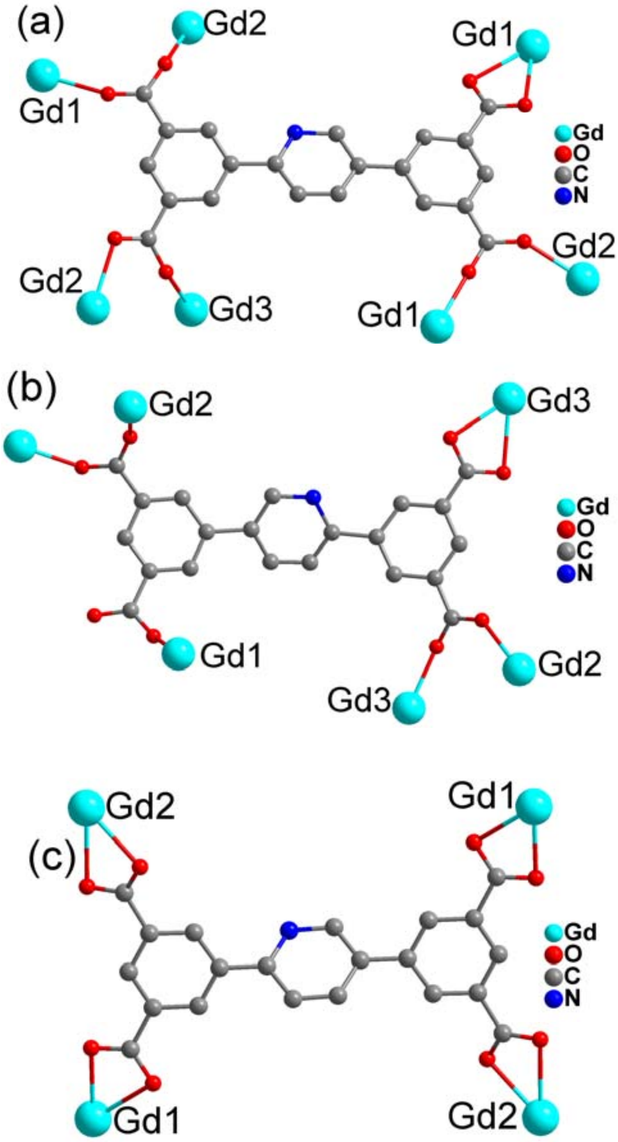

Fig. S2 The coordination modes of the crystallographically independent L^{4-} and HL^{3-} ligands. (Hydrogen atoms are omitted for clarity).

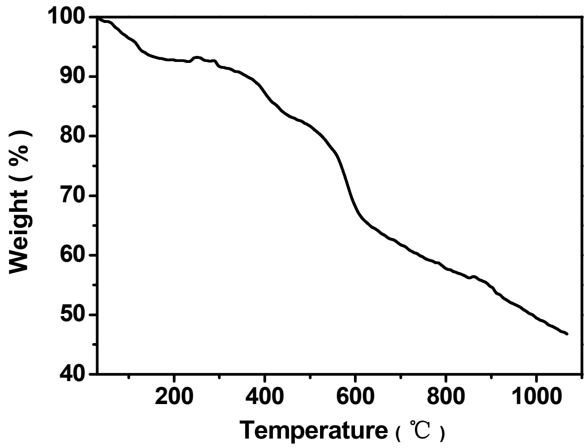

Fig. S3 Thermogravimetric analyses of compound **1**. For **1**, the two-step weight loss before 300 °C corresponds to the release of lattice water molecules and coordinated water molecules and other solvent molecules, and the following weight losses correspond to the decomposition of compound **1**.

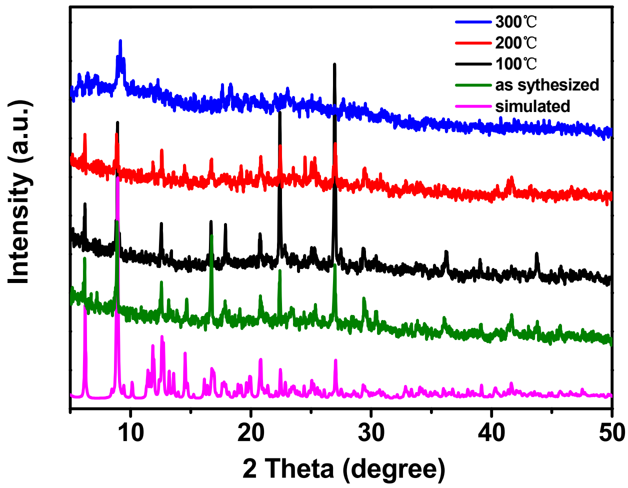

Fig. S4 The powder X-ray diffraction (PXRD) patterns for **1** and **1** heated at 100 °C, 200 °C and 300 °C in the muffle furnace. (under the air atmosphere)

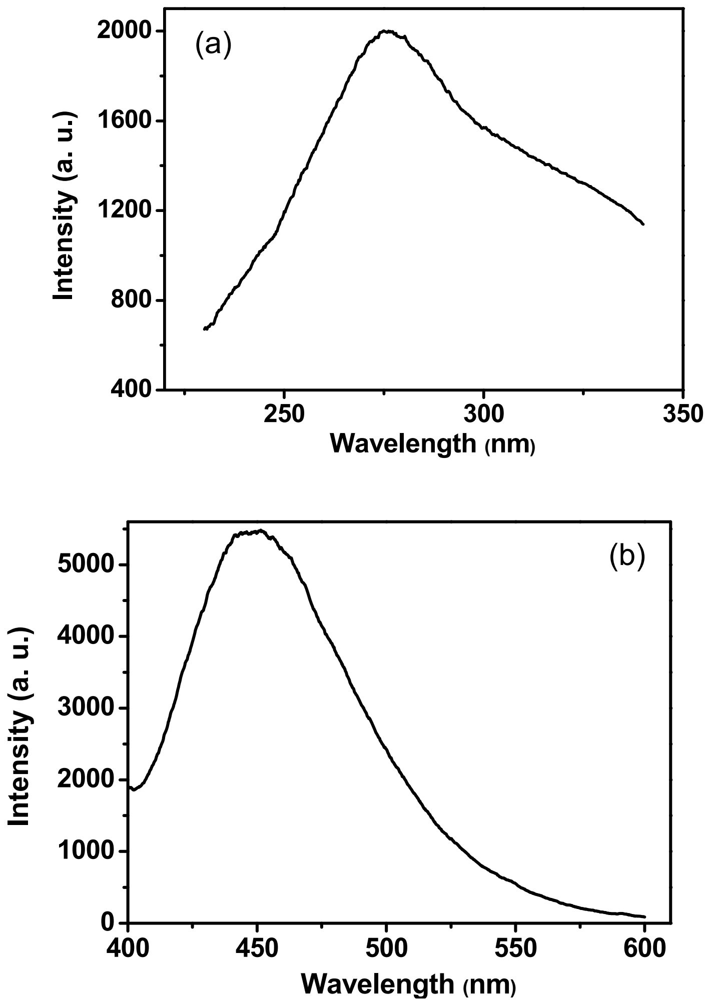

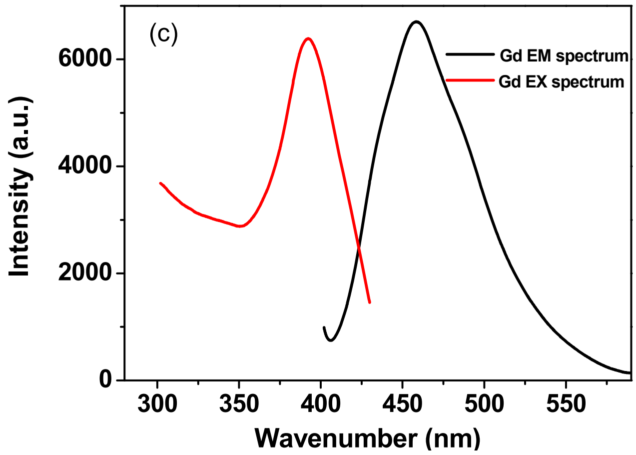

Fig. S5 (a) The solid-state excitation spectra of free H_4L ligands at room temperature (λ_{em} = 275 nm); (b) The solid-state emission spectra of free H_4L ligands at room temperature, λ_{ex} = 392 nm; (c) The solid-state excitation spectra (λ_{em} = 459 nm) and emission spectra (λ_{ex} = 392 nm) of **1** at room temperature.

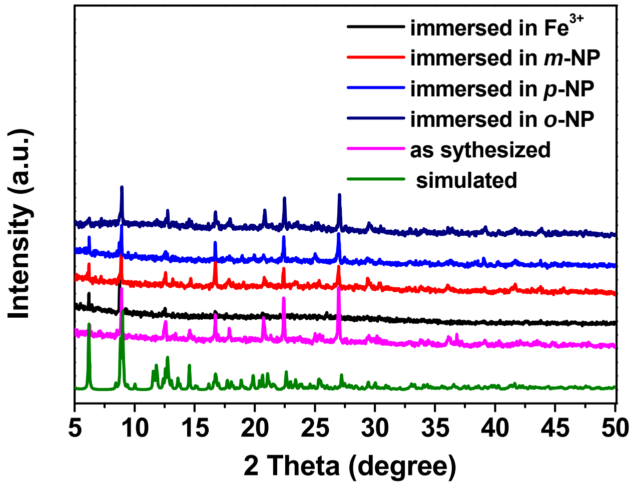

Fig. S6 The powder X-ray diffraction (PXRD) patterns for **1** and **1** immersed in 0.1 M aqueous solutions of *o*-NP, *m*-NP, *p*-NP and Fe^{3+} ions.

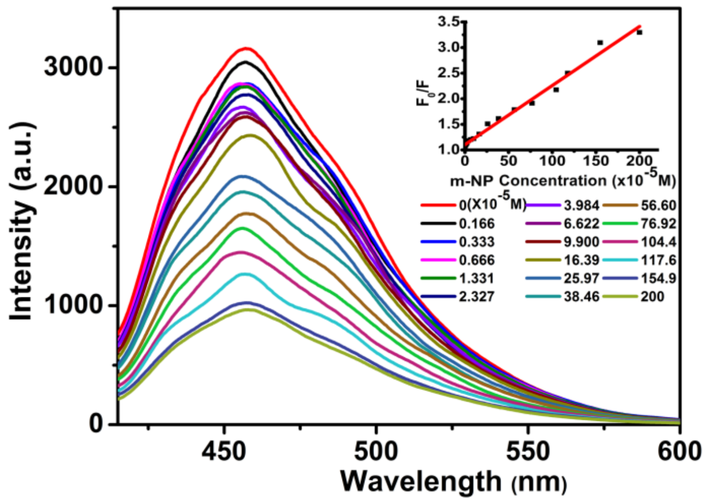

Fig. S7 Effect on the emission spectra of **1** dispersed in water upon incremental addition of a

m-NP aqueous solution (λ_{ex} = 392 nm). Inset: Stern-Volmer plot of F_0/F versus the m-NP concentration.

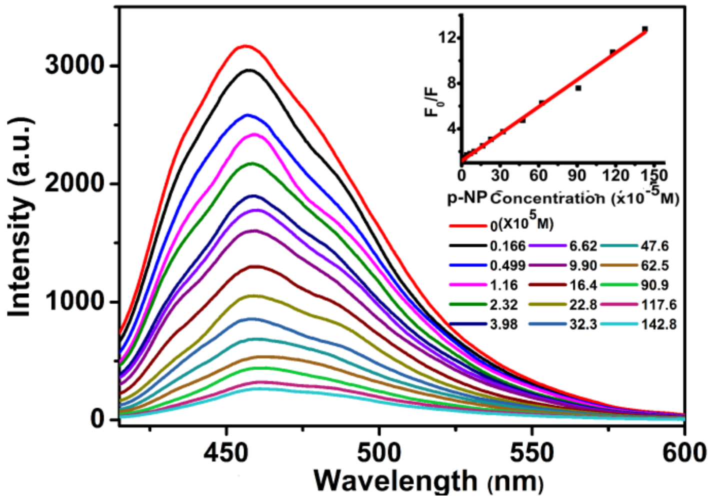

Fig. S8 Effect on the emission spectra of **1** dispersed in water upon incremental addition of a p-NP aqueous solution (λ_{ex} = 392 nm). Inset: Stern-Volmer plot of F_0/F versus the p-NP concentration.

The detection limits were the minimum detectable concentration. In our luminescence titration experiment, the minimum detectable concentrations were 1.67 ppm for o-NP, m-NP and p-NP.

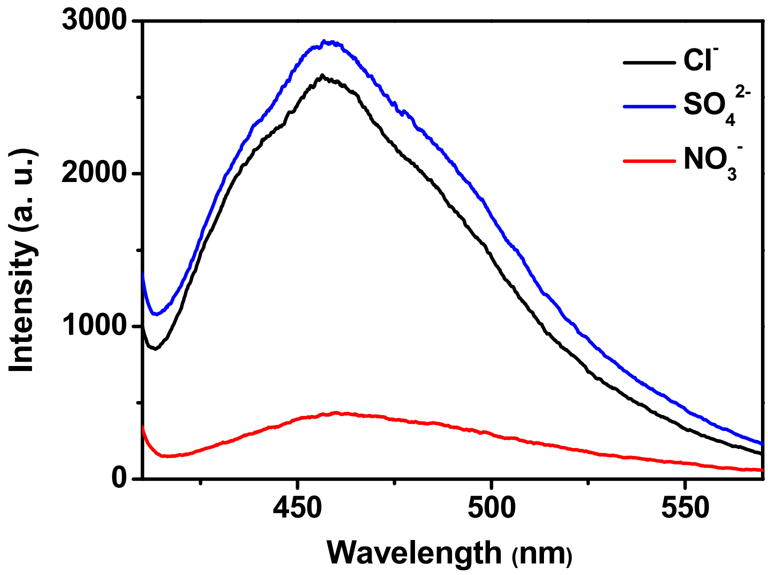

Fig. S9 Fluorescence intensity for **1** dispersed in aqueous solution of $FeCl_3{\cdot}6H_2O$, $Fe_2(SO_4)_3$ $Fe(NO_3)_3{\cdot}9H_2O$ (0.01 M).

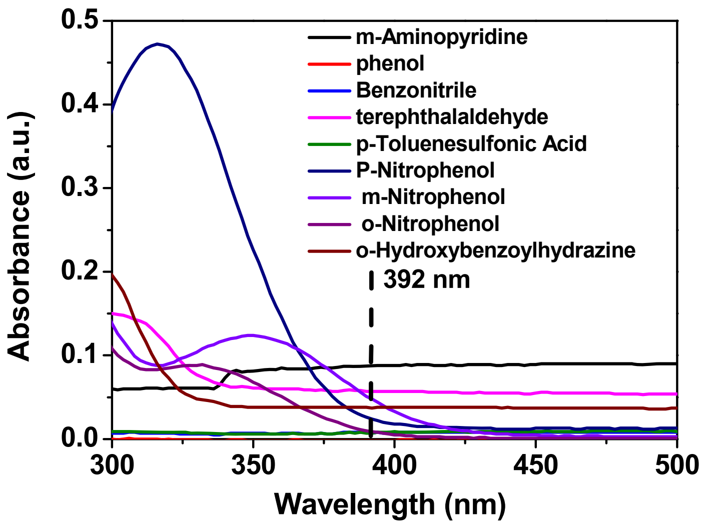

Fig. S10 The UV-Vis absorption spectrum of selected small organic molecules.

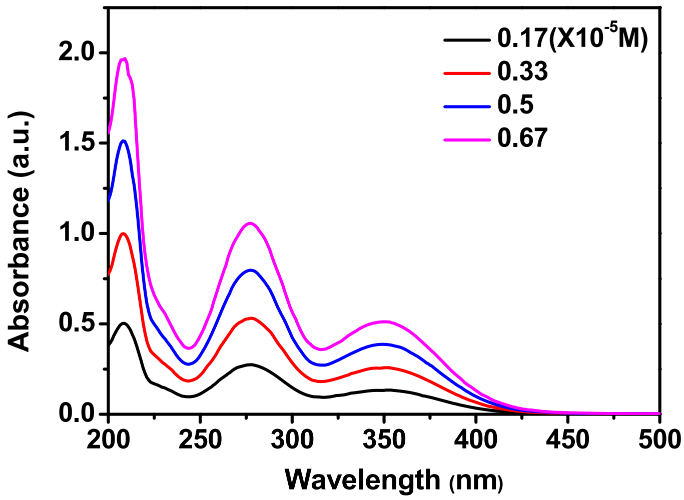

Fig. S11 The UV-Vis absorption spectrum of **1** dispersed in water upon increasing addition of a *o*-NP aqueous solution.

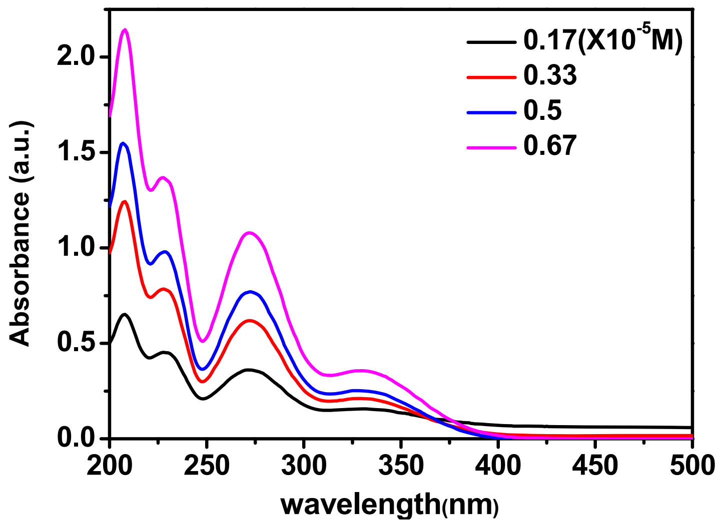

Fig. S12 The UV-Vis absorption spectrum of **1** dispersed in water upon increasing addition of a *m*-NP aqueous solution.

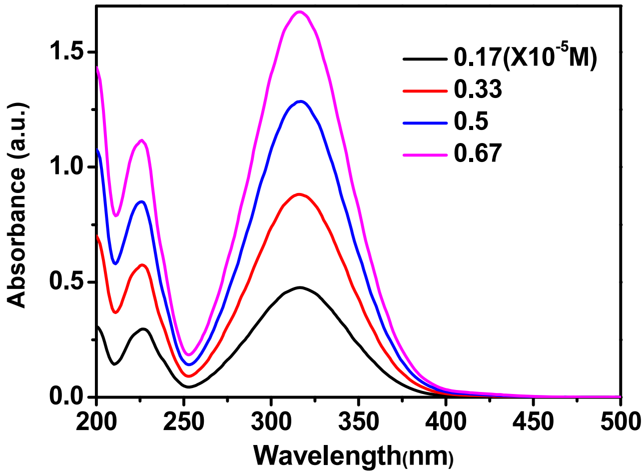

Fig. S13 The UV-Vis absorption spectrum of **1** dispersed in water upon increasing addition of a *p*-NP aqueous solution.

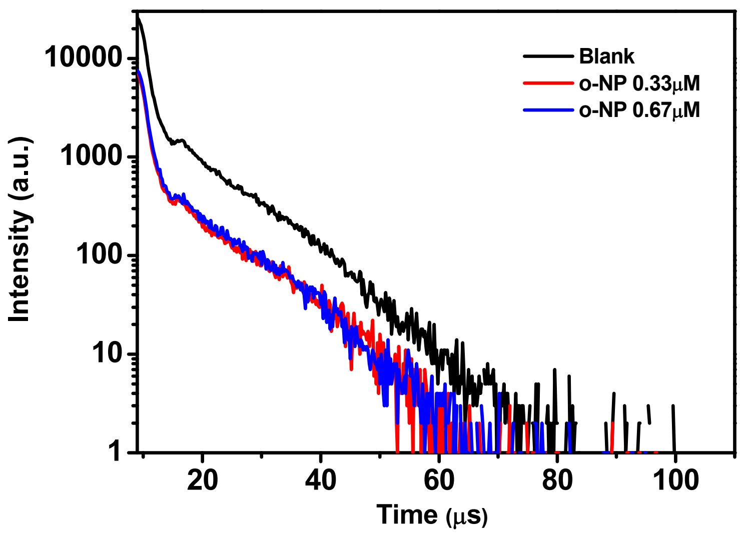

Fig. S14 Semilog plots of fluorescence decay versus time in different concentrations of *o*-NP, excited and monitored at 392 and 459 nm, respectively.

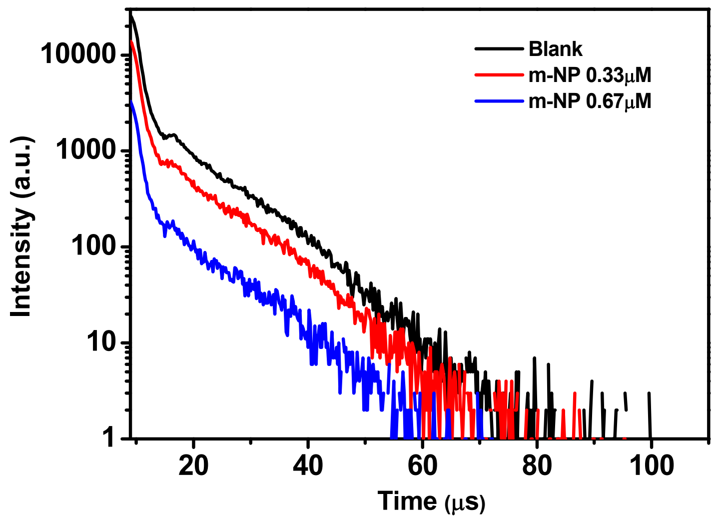

Fig. S15 Semilog plots of fluorescence decay versus time in different concentrations of *m*-NP, excited and monitored at 392 and 459 nm, respectively.

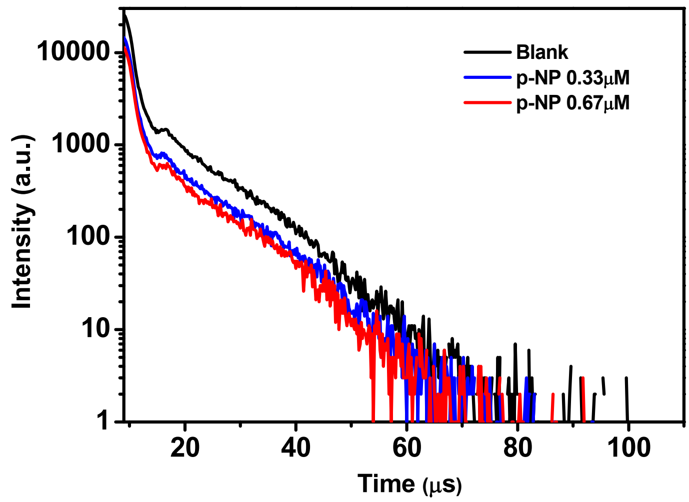

Fig. S16 Semilog plots of fluorescence decay versus time in different concentrations of *p*-NP, excited and monitored at 392 and 459 nm, respectively.

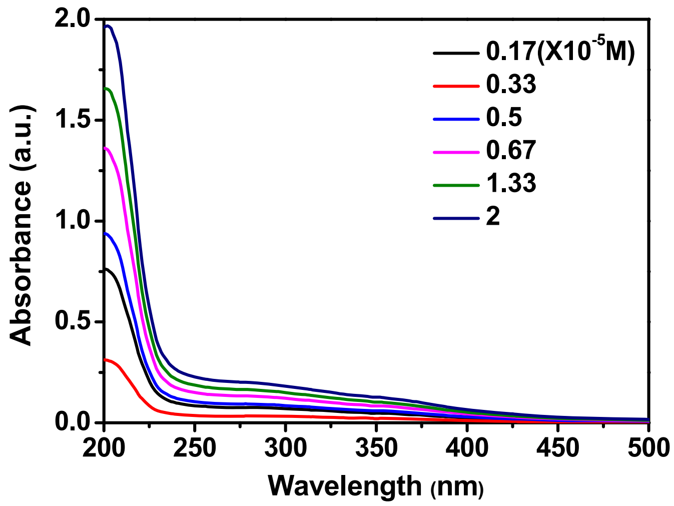

Fig. S17 UV-Vis absorption spectrum of **1** dispersed in water upon increasing addition of a Fe^{3+} aqueous solution.

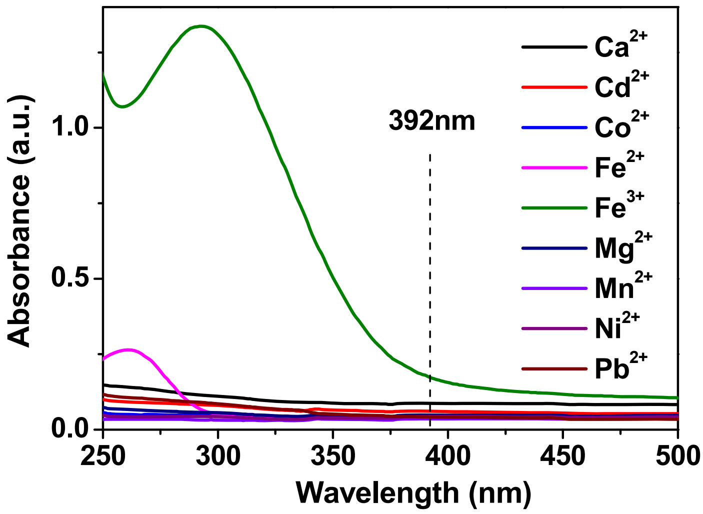

Fig. S18 The UV-Vis absorption spectrum of the selected 0.01 M different M^{z+} (Cd^{2+}, Ca^{2+}, Co^{2+}, Fe^{2+}, Fe^{3+}, Mg^{2+}, Mn^{2+}, Ni^{2+} and Pb^{2+}) ions aqueous solution.